condensed matter

MDPI

*Article*

# Superconductivity and the Jahn–Teller Polaron

**Annette Bussmann-Holder [1] and Hugo Keller [2,*]**

[1] Max-Planck-Institute for Solid State Research, Heisenbergstr. 1, D-70569 Stuttgart, Germany; a.bussmann-holder@web.de or a.bussmann-holder@fkf.mpg.de
[2] Physik-Institut, Universität Zürich, Winterthurerstr. 190, CH-8057 Zürich, Switzerland
* Correspondence: keller@physik.uzh.ch

**Abstract:** In this article, we review the essential properties of high-temperature superconducting cuprates, which are unconventional isotope effects, heterogeneity, and lattice responses. Since their discovery was based on ideas stemming from Jahn–Teller polarons, their special role, together with the Jahn–Teller effect itself, is discussed in greater detail. We conclude that the underlying physics of cuprates cannot stem from purely electronic mechanisms, but that the intricate interaction between lattice and charge is at its origin.

**Keywords:** high-temperature cuprate superconductors; superconductivity; Jahn–Teller effect; polarons

## 1. Introduction

Since the discovery of high-temperature superconductivity (HTSC) in the La-Ba-Cu-O system by J.G. Bednorz and K.A. Müller in 1986 [1], 35 years ago, the search for room-temperature superconductivity has been enormously intensified. However, not only experimental efforts are at play, but, theoretically, this discovery has also been taken as evidence that BCS theory needs to be abandoned and new pairing mechanisms are required. In this article, we provide a short review of conventional (before 1986) and unconventional (after 1986) superconductors and concentrate on the Jahn–Teller polaron (JTP) concept, the idea behind the 1986 discovery. We focus on the direct, observable consequences of the JTP and possible outlooks for future HTSC research.

## 2. Superconductiviy before 1986

As is well known, superconductivity was discovered in 1911, more than a century ago, by Heike Kammerlingh Onnes, together with his assistant, Gilles Holst, in ultra-pure mercury. This discovery was accidental and caused by curiosity, namely regarding the behavior of the resistivity of metals at low temperatures. Since Kammerlingh Onnes had made important progress to liquefy helium, he wished to determine which properties of metals can be explored at low temperatures. At that time, there were several theories predicting the temperature dependence of the resistivity of metals at ultra-low temperatures. In view of the inability to reach this temperature scale, the true dependence remained speculative only. Kammerlingh Onnes reached 4 K with He liquefaction and chose mercury for his experiments, since this was available in ultra-pure form, i.e., free of impurities. The major surprise was that the resistivity of Hg dropped to zero at 4.2 K, which was later named superconductivity. Kammerlingh Onnes received the Nobel Prize for Physics in 1913—not, as frequently believed, for the discovery of superconductivity, but for the liquefaction of the last gas, helium.

After this breakthrough discovery, further elemental metals were found to be superconducting as well, all in the low-temperature regime below 7 K. Only in 1933 was a further characteristic effect of superconductors discovered by Meissner and Ochsenfeld, who showed that superconductors expel a magnetic field completely from the interior.

check for updates

**Citation:** Bussmann-Holder, A.; Keller, H. Superconductivity and the Jahn–Teller Polaron. *Condens. Matter* **2022**, *7*, 10. https://doi.org/10.3390/condmat7010010

Academic Editors: Carmine Attanasio and Mona Berciu

Received: 1 December 2021
Accepted: 12 January 2022
Published: 20 January 2022

**Publisher's Note:** MDPI stays neutral with regard to jurisdictional claims in published maps and institutional affiliations.

Further important discoveries for the development of a theory for superconductivity by Bardeen, Cooper and Schrieffer (BCS) were the isotope effect and the concept of paired electrons, namely the formation of Cooper pairs. Both together were finally the basis for the BCS theory of phonon-mediated superconductivity [2,3].

In 1950, two independent research groups observed an isotope effect (IE) on the superconducting transition temperature $T_c$ of mercury [4,5], which played a crucial role in the development of a theoretical microscopic model of superconductivity—in particular, of the weak-coupling BCS theory, where the electron–phonon interaction is the paring glue for Cooper pairs [2,3]. The isotope shift on $T_c$ can be quantified by the following relation:

$$T_c \propto M^{-\alpha}, \quad \alpha = -d \ln T_c / d \ln M, \tag{1}$$

where $M$ is the isotope mass, and $\alpha$ is the IE exponent. In the framework of weak-coupling BCS theory, $T_c \propto M^{-1/2}$ with $\alpha_{\mathrm{BCS}} \simeq 0.5$. For many conventional superconductors, values of $\alpha \approx 0.5$ were found (Pb: $\alpha = 0.48$, Hg: $\alpha = 0.50$, Sn: $\alpha = 0.47$). However, values much lower than 0.5 were also reported, e.g., Os ($\alpha = 0.20$) or Ru and Zr ($\alpha \simeq 0$). Note, however, that a zero IE does not mean that no lattice effects are involved in the pairing. We come back to this important point later when we discuss isotope effects in cuprate superconductors.

In conclusion, the observation of an IE in conventional superconductors offers strong support of the concept of BCS theory, where the electron–phonon interaction leads to Cooper pairing.

## 3. The Jahn–Teller Effect

The discovery of high-temperature superconductivity by J.G. Bednorz and K.A. Müller [1] was based on three important aspects related to cuprates and oxides: (1) $Cu^{2+}$ is a strong Jahn–Teller (JT) ion; (2) superconductivity in oxides was rather rare; however, if found, their transition temperatures were unexpectedly high, despite the fact that the density of states was low and the ratio of phonon frequency versus Fermi energy close to one; (3) this observation led to the conclusion that the electron–lattice interaction is unusually large. The introduction of the JT polaron offered an explanation for the above and was taken as a possible route in the search for new oxide superconductors. For this reason, both the JT concept and the JT polaron are discussed in further detail in the following.

The JT effect was predicted and explained by Jahn and Teller at the Washington Physical Society Meeting in 1936 [6,7]: *As a general rule the electronic state of a polyatomic molecule can be degenerate only if the atomic configuration has a sufficiently high degree of symmetry. If the atomic nuclei are displaced the degenerate state may split up and if the splitting is a linear function of the displacement the original symmetrical configuration, and with it the original degenerate state, does not correspond to an equilibrium state of the molecule.*

The principal statement in this work is that stability of a molecule and electronic degeneracy are not possible simultaneously unless the molecule is linear. Therein, they consider all possible types of symmetry of the molecule by applying group-theory symmetrical rules (Jahn–Teller theorem, JTT): *All non-linear nuclear configurations are therefore unstable for an orbitally degenerate state*. This statement holds as long as the electrons contribute appreciably to the molecular binding. The central issue of the theorem is that ionic displacements and electronic motion cannot be decoupled, but form a novel vibronic state. This implies that the Born–Oppenheimer approximation fails in systems with JT active centers, and it is no more possible to separate the electronic wave function from the ionic one. This is very reminiscent of the polaron problem.

Early on, the group around H. Thomas suggested that a JT polaron might form in itinerant electron systems [8] (Höck, Nickisch, and Thomas, HNT), which laid the groundwork for the discovery of cuprate superconductors [1]. This theory will be discussed in more detail in the following. As already mentioned above, the JTT states that the interaction of an orbitally degenerate electronic state with the vibrational lattice modes destabilizes the lattice and leads to a lower symmetry of the latter, i.e., a structural phase transition. For a cooperative JT effect to occur, typically, insulators are considered, whereas HNT [8]

postulated that the JT effect might also occur in certain metals—the band JT mechanism. They considered a simplified case where a single electron with double degeneracy moves in a lattice where a strong electron–lattice interaction is present, meaning that the electron contributes to the binding of the molecule. The electron is allowed to hop from site to site and interacts with a symmetry-breaking lattice coordinate. This is in contrast to conventional electron–lattice coupling, where the interaction is caused by a fully symmetric one. The energy gain and JT stabilization energies proportional to the interaction divided by the lattice energy can reach substantial values. The case of interest for HNT [8] is where the electronic band width and the JT energy are comparable. If the coupling is then strong enough, the electron becomes trapped, i.e., localizes, and only together with the surrounding lattice cloud can move in total through the lattice. A JT polaron is formed.

The study by HNT [8] assumes that a molecular complex of tetragonal symmetry is realized in the crystalline unit cell with two-fold degenerate orbital states $\Psi_{l1}, \Psi_{l2}$ at lattice site $l$, which form bands of local doublets. Competition between electron transfer and localization arises when the electron–phonon interaction is switched on. Localization is realized for strong electron–lattice coupling, whereas, in the weak-coupling limit, band formation is favored.

In order to quantify these properties, the Hamiltonian $H_{pol}$ has to consist of at least three terms [8]:

$$H_{pol} = H_{el} + H_{latt} + H_{JT} \tag{2}$$

with

$$H_{el} = \varepsilon_0 \sum_l (c_{l1}^+ c_{l1} + c_{l2}^+ c_{l2}) - \frac{1}{2} \sum_{l,l',\gamma} t_\gamma(l,l')\, c_{l\gamma}^+ c_{l'\gamma} \ , \ \gamma = 1,2 \tag{3}$$

$$H_{latt} = \sum_l (p_l^2/2M + \frac{1}{2} M\omega_0^2 Q_l^2) - \frac{1}{2} \sum_{l,l'} V_{l,l'} Q_l Q_{l'} \tag{4}$$

$$H_{JT} = -g \sum_l Q_l (n_{l1} - n_{l2}) \tag{5}$$

$c^+, c$ are electron creation and annihilation operators with $c^+c = n$ and site energy $\varepsilon_0$. $t$ is the hopping integral, which is effective only for states of the same symmetry, i.e., inter-orbital hopping is neglected, in accordance with symmetry considerations. The lattice Hamiltonian $H_{latt}$ consists of the momentum $p$ and conjugate displacement coordinate $Q$ and an intersite potential $V$, which couples nearest neighbor sites and accounts for an optic mode. Otherwise, any dispersion is suppressed, since an Einstein oscillator with frequency $\omega_0$ is assumed. The electron–lattice interaction proportional to $g$, as given by $H_{JT}$, couples the electrons at site $l$ to the symmetry-breaking displacement coordinate at the same site. The Jahn–Teller energy $E_{JT} = -g^2/2M/\omega_0^2$ is typically much stronger than conventional electron–lattice interaction terms. The interesting problem of this scenario is realized when the Jahn–Teller energy $E_{JT}$ is of the same order of magnitude as the hopping integral $t$, since, in this situation, it can be expected that the electron travels with its surrounding displacement cloud through the lattice, thus forming a JT polaron. The total object is characterized by its momentum $k$ and site index $l$, which are replaced by a single index $l$ in the following in order to keep the equations more transparent. Introducing phonon creation and annihilation operators $b^+, b$, a trial translationally invariant wave function for the combined electron–lattice is given by:

$$|\Psi_k\rangle = A \sum_l \exp(ikR_l) \prod_{l'} \exp[\alpha_{l,l'}(k)(b_{l'}^+ - b_l)] \sum_{l'} a_{l,l'}^{(k)}\, c_{l'}^+ |0\rangle \ , \tag{6}$$

where $A$ is a normalization constant, and $\alpha$ is the shape of the total deformation, whereas $a$ determines the form of the electron wave packet. Both quantities $A$ and $a$ are variational parameters.

The main results are that a wave packet of the form $\sum_{l''} a^{(k)}_{l-l''} c_{l''}|0\rangle$ refers to localized states when its width is small and is located near the lattice site $l$ with a deformation given by $\alpha^{(k)}_{l-l'}$. This limit refers to $E_{JT} \gg t, \hbar\omega_0$ . In the opposite limit, namely $\alpha^{(k)}_{l-l'}$ being small, the state $|\Psi_k\rangle$ corresponds to an almost freely moving electron, which is nearly unaffected by the lattice. However, if $\alpha^{(k)}_{l-l'} = a = \text{const.}$, then $|\Psi_k\rangle$ represents the combined electron–lattice bound state, where a momentum-independent electron couples to a phonon with momentum $k$. In order to obtain an approximate ground-state energy $E^{(0)}_k$, minimization with respect to $A$ and $\alpha^{(k)}_{l-l'}$ has to be carried through.

The above problem has been solved for a 1D chain where ion–ion interactions ($\approx V_{l,l'}$) are suppressed, the electron hopping is restricted to nearest neighbors and the lattice spectrum consists of an Einstein oscillator. The ground-state energy for the Jahn–Teller polaron is then given by:

$$E^{(0)}_k = E^{(0)}_0 + \frac{\hbar^2 k^2}{2m_{eff}}\ , \tag{7}$$

with $m_{eff}$ being enlarged as compared to the bare electronic mass. Limiting cases of this simplified model yield, however, the relevant physics of the problem as outlined above, namely $E_{JT} \ll t$. The distortion due to the coupling to the electronic motion is small and the electron motion through the lattice is almost unaffected, i.e., free-electron-like. With increasing JT energy, the distortion also increases, and for $E_{JT} \gg t$, an isolated JT molecular complex results. The competition between localization and itineracy is thus an inherent property of the JT polaron problem.

One might ask, what is the distinction between the "conventional" Holstein-type polaron [9–11] and the JT polaron [8]? While, in the former case, a fully symmetric distortion pattern is formed, in the latter, a distorted lattice is involved. In addition, in the first case, electronic degeneracy is not a prerequisite, whereas, in the JT scenario, it is necessary, since the lifting of the degeneracy causes an important energy gain. Related to the Lang–Firsov transformation [12], a variational ansatz is made, where analogous effects on the electronic and vibrational states are obtained—namely, the electronic wave function (kinetic energy) is exponentially renormalized by the lattice, whereas the lattice energy experiences a rigid shift due to the coupling to the degenerate electronic state.

With respect to cuprates, limitations of the applicability of the JTT are readily apparent: namely, the superconducting cuprates are doped materials. Correspondingly, the valency of the copper ion is not unique, but changes inhomogenously within the system. Thus, depending on the local copper valency, a JT effect might be possible or not. In addition, the changing valency of copper goes hand in hand with lattice responses, inducing locally distorted regions in coexistence with undistorted ones. From the above, the most important message is that heterogeneity coupled with lattice responses is intrinsic and essential to cuprate superconductivity. This aspect has been emphasized early on by K.A. Müller [13], and, in conjunction with poorly understood experiments, he suggested that cuprates do not have a single $d$-wave order parameter, but that two coupled-order parameters with $s + d$ symmetry need to be considered [14].

## 4. Heterogeneities and Mixed-Order Parameters in Cuprate Superconductors

Clear experimental evidence for intrinsic heterogeneity in the cuprates has been given by extended X-ray absorption fine structure (EXAFS) spectroscopy and pair distribution function analysis, where a stripe-like ordering of these regions has been detected [15]. Again, it must be concluded that, in view of the symmetry lowering in the distorted regions, charge-rich areas and the fully symmetric undistorted charge-poor regions occur, where, in the latter, the efficiency of the JT effect as a global player is absent. However, the strong lattice responses observed experimentally cannot be ignored in a theoretical approach of cuprate superconductivity, and various suggestions have been made that polaron physics and bipolaron pairing scenarios are relevant for its understanding [11,16].

In the majority of the community, it is assumed that cuprate superconductors have a pure $d$-wave order parameter (see, e.g., [17–19]). However, based on experimental findings and theoretical considerations, K.A. Müller proposed that cuprate superconductors must have a mixed $s + d$-order parameter [14,20] (see above) that reflects the intrinsic inhomogeneities (hole-rich and hole-poor stripe-like regions) in these systems [13]. In order to test this scenario, detailed muon-spin rotation ($\mu$SR) experiments on various families of cuprate superconductors were performed, since, with this technique, it is possible to directly measure the magnetic penetration depth (superfluid density) and its temperature dependence, which provides unique clues for $s$-, respectively, $d$-wave order parameters [21–23].

The $\mu$SR technique is a powerful and highly sensitive tool for investigating the magnetic properties of superconductors and magnetic systems. The positive muon $\mu^+$ (spin $S = 1/2$) serves as a microscopic magnetic probe to detect local magnetic fields in the bulk of a solid, even with no external magnetic field applied (zero-field $\mu$SR). This bulk sensitivity makes $\mu$SR superior to APRES and STM, which are surface-sensitive and do not probe the bulk properties of the sample. We will discuss this important point later. Moreover, in contrast to most standard experimental techniques (e.g., neutron scattering, NMR, ARPES), $\mu$SR allows us to determine the magnetic volume fraction in a sample, which is unique and of particular relevance for cuprates and related systems (e.g., coexistence of superconductivity and magnetism). $\mu$SR has provided important information on the microscopic magnetic properties of these materials, which are difficult to obtain with any other experimental technique. Some examples are:

- Direct determination of the local magnetic field distribution $p(B)$ and the magnetic penetration depth in type II superconductors;
- Study of the complex vortex-phase diagram (flux–lattice melting, 3D–2D crossover, vortex fluctuations) of cuprate superconductors;
- Coexistence of superconductivity and magnetism (magnetic phase diagram) in cuprate and iron-based superconductors;
- Detection of spontaneous magnetic fields (orbital currents) in the pseudogap phase of cuprate superconductors;
- Study of spin stripe order in cuprate systems.

$\mu$SR is an ideal method to determine the pairing symmetry ($s$, $d$, $s + d$, etc.) of a cuprate superconductor in the bulk of a single-crystal sample by measuring the temperature dependence of the magnetic penetration depths (superfluid densities) $\lambda_a$, $\lambda_b$ and $\lambda_c$ along the three principal crystallographic axes, $a$, $b$ and $c$. Such experiments were performed on three different cuprate systems, $La_{1.83}Sr_{0.17}CuO_4$ [21], $YBa_2Cu_3O_{7-\delta}$ [22] and $YBa_2Cu_4O_8$ [23], in order to demonstrate that the observed behavior is generic for cuprates, which indeed was found to be the case.

As an example, Figure 1 shows the temperature dependences of the $\mu$SR relaxation rates $\sigma_a \propto \lambda_a^{-2}$, $\sigma_b \propto \lambda_b^{-2}$ and $\sigma_c \propto \lambda_c^{-2}$ of single-crystal $YBa_2Cu_3O_{7-\delta}$ [22]. Note that $\sigma_c(T) \propto \lambda_c^{-2}(T)$ is consistent with a pure $s$-wave order parameter, in agreement with $c$-axis tunneling experiments [24]. However, both $\sigma_a(T) \propto \lambda_a^{-2}(T)$ and $\sigma_b(T) \propto \lambda_b^{-2}(T)$ show a characteristic "up-turn" at a low temperature. A theoretical analysis of the data with a phenomenological model of a coupled $s + d$-wave order parameter [25] reveals that, in the $CuO_2$ plane, a small $s$-wave order parameter (small gap) coexists with a dominant $d$-wave order parameter (large gap); the contribution of the $d$-wave gap to the total in-plane superfluid density is ≈75% [22]. This behavior is generic for all cuprate superconductors investigated [21–23], and also manifests the intrinsic inhomogeneity of the cuprates [13,26].

Several experimental studies using various techniques (e.g., ARPES, phase-sensitive tunneling experiments, NMR, $\mu$SR, magnetization experiments, etc.) were conducted to test the pairing symmetry in cuprate superconductors. However, controversial results concerning the gap symmetry ($d$, $s$, $s + d$) were obtained [20]. This is due to the fact that some techniques (ARPES, phase-sensitive tunneling, etc.) probe the gap symmetry near the surfaceof the sample, whereas other methods ($\mu$SR) probe the order parameter in the bulk of the sample. Based on these experimental findings and group theoretical

considerations, K.A. Müller [26,27] proposed that the order parameter has a mixed $s + d$ symmetry, changing from a dominant $d$-wave character near the surface to a more $s$-wave character in the bulk of the superconductor. This scenario of coexisting $s + d$ order parameters is clearly supported by recent AC magnetization and $\mu$SR studies of the in-plane ($\lambda_{ab}$) and out-of-plane ($\lambda_c$) magnetic field penetration depths near the surface and in the bulk of the electron-doped cuprate superconductor $Sr_{0.9}La_{0.1}CuO_2$ [28].

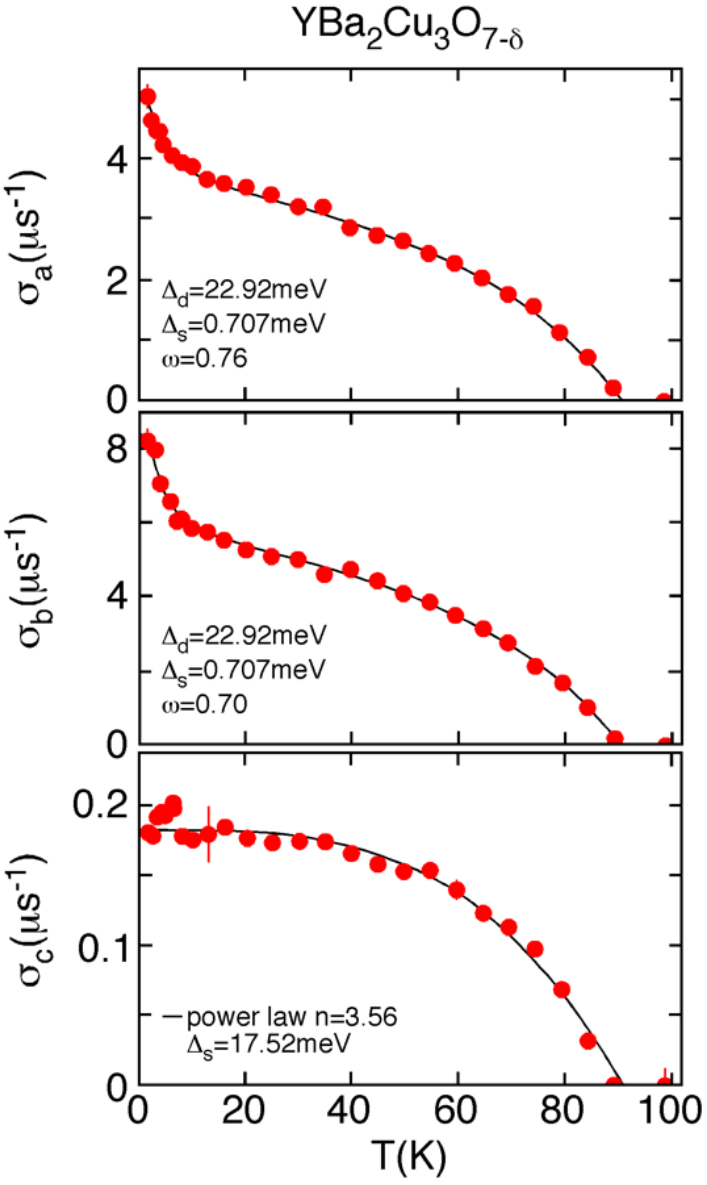


**Figure 1.** Temperature dependences of the $\mu$SR relaxation rates $\sigma_a \propto \lambda_a^{-2}$, $\sigma_b \propto \lambda_b^{-2}$ and $\sigma_c \propto \lambda_c^{-2}$ of single-crystal $YBa_2Cu_3O_{7-\delta}$ measured along the principal crystallographic axes $a$, $b$ and $c$. The solid lines are the results of model calculations described in [22]. (Reprinted with permission from Ref. [22]. Copyright 2007 APS).

## 5. The Two-Band Model

The above-described experimental data can be modeled by a two-band extended BCS Hamiltonian, where both bands are characterized by different pairing symmetries. The Hamiltonian $H_{TB}$ for the two-band model in its simplest form reads [29,30]:

$$H_{TB} = H_0 + H_1 + H_2 + H_{12} \quad (8)$$

with

$$H_0 = \sum_{k_1,\sigma} \epsilon_{k_1}\, c^+_{k_1\sigma}\, c_{k_1\sigma} + \sum_{k_2,\sigma} \epsilon_{k_2}\, d^+_{k_2\sigma}\, d_{k_2\sigma}\ , \tag{9}$$

where $\epsilon_{k_i}$ is the band energy $\epsilon_k = \tilde{\varepsilon} - \varepsilon_k - \mu$, and $\tilde{\varepsilon_i}$ denotes the position of the $c$ and $d$ in bands $i = 1,\ 2$, and $c^+,\ c,\ d^+,\ d$ are electron creation and annihilation operators in band 1, 2, with spin index $\sigma$. The interband and intraband interactions $H_i$ and $H_{12}$ are explicitly given by [29,30]:

$$H_1 = -\sum_{k_1,k_1',q} V_1(k_1,k_1')\, c^+_{k_1+q/2\uparrow}\, c^+_{-k_1+q/2\downarrow}\, c_{-k_1'+q/2\downarrow}\, c_{k_1'+q/2\uparrow} \tag{10}$$

$$H_2 = -\sum_{k_2,k_2',q} V_2(k_2,k_2')\, d^+_{k_2+q/2\uparrow}\, d^+_{-k_2+q/2\downarrow}\, d_{-k_2'+q/2\downarrow}\, d_{k_2'+q/2\uparrow} \tag{11}$$

$$H_{12} = -\sum_{k_1,k_2,q} V_{12}(k_1,k_2)\, [c^+_{k_1+q/2\uparrow}\, c^+_{-k_1+q/2\downarrow}\, d_{-k_2+q/2\downarrow}\, d_{k_2+q/2\uparrow} + h.c.] \tag{12}$$

By performing a BCS mean-field analysis of the above equations, the gap equations are derived and the superconducting transition temperature evaluated self-consistently. After applying standard techniques, one obtains:

$$\langle c^+_{k_1\uparrow}\, c^+_{-k_1\downarrow}\rangle = \frac{\bar{\Delta}^*_{k_1}}{2E_{k_1}} \tanh\frac{E_{k_1}}{2k_BT} = \bar{\Delta}^*_{k_1}\,\Phi_{k_1} \tag{13}$$

$$\langle d^+_{k_2\uparrow}\, d^+_{-k_2\downarrow}\rangle = \frac{\bar{\Delta}^*_{k_2}}{2E_{k_2}} \tanh\frac{E_{k_2}}{2k_BT} = \bar{\Delta}^*_{k_2}\,\Phi_{k_2} \tag{14}$$

with $E^2_{k_1} = \epsilon^2_{k_1} + |\bar{\Delta}_{k_1}|^2$, $\bar{\Delta}_{k_1} = \Delta_{k_1} + A_{k_1}$ and $E^2_{k_2} = \epsilon^2_{k_2} + |\bar{\Delta}_{k_2}|^2$, $\bar{\Delta}_{k_2} = \Delta_{k_2} + B_{k_2}$, which results in the following self-consistent set of gap equations:

$$\bar{\Delta}_{k_1} = \sum_{k_1'} V_1(k_1,k_1')\,\bar{\Delta}_{k_1'}\,\Phi_{k_1'} + \sum_{k_2} V_{12}(k_1,k_2)\,\bar{\Delta}_{k_2}\,\Phi_{k_2} \tag{15}$$

$$\bar{\Delta}_{k_2} = \sum_{k_2'} V_2(k_2,k_2')\,\bar{\Delta}_{k_2'}\,\Phi_{k_2'} + \sum_{k_2} V_{12}(k_1,k_2)\,\bar{\Delta}_{k_1}\,\Phi_{k_1} \tag{16}$$

from which the temperature dependencies of the two gaps (Figure 2a) and the superconducting transition temperature $T_c$ have to be determined [31]. The effect of the interband coupling on $T_c$ is demonstrated in Figure 2b for the case of two isotropic $s$-wave gaps (green circles) and the combination of $s + d$ symmetry (blue circles), where a substantial increase in $T_c$ takes place as compared to the $s + s$ case. The largest effect on $T_c$ is, however, clearly due to the interband interaction itself, which rapidly changes the system from non-superconducting ($V_{12} = 0$) to finite values of $T_c$ (Figure 2b).

The above-described model has been used to calculate the penetration depth and compared to results obtained experimentally, with apparently very good agreement with the experiment [25].

A further challenge of the above modeling is the understanding of the unconventional isotope effects observed in cuprates. These are presented in the following.

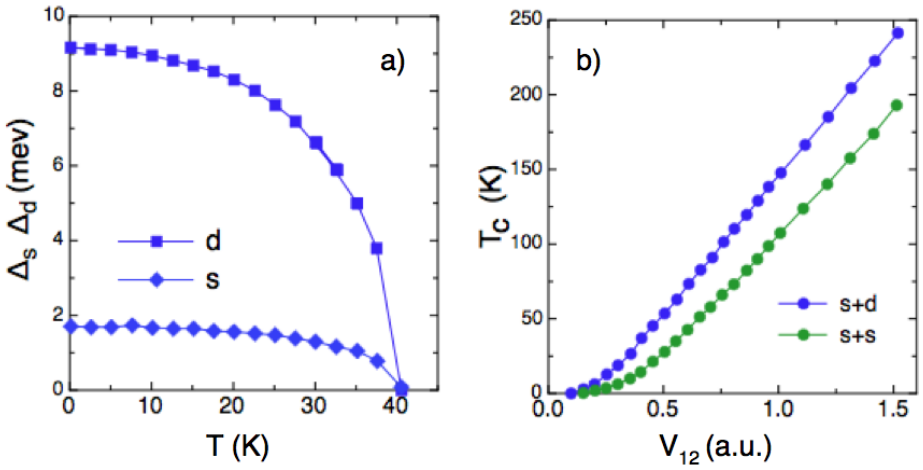


**Figure 2.** (**a**) Self-consistently derived coupled gaps with *s*- (blue diamonds) and *d*-wave symmetry (blue squares) with interband coupling $V_{12} = 0.4$. (**b**) Superconducting transition temperature $T_c$ as a function of the interband interaction $V_{12}$. The green circles refer to $s + s$, and the blue circles to $s + d$ pairing symmetry. (After [31]).

## 6. Unconventional Isotope Effects in Cuprate Superconductors

The discovery of high-temperature superconductivity in the cuprates [1] with transition temperatures $T_c \simeq 100$ K, much higher than for conventional low-temperature superconductors, raised some fundamental questions: What is the origin of the electron–hole pairing mechanism in these superconductors? Is it the electron–phonon pairing as in conventional superconductors, or are purely electronic effects at play? In order to explore the origin, an oxygen ($^{16}O/^{18}O$)-isotope effect (OIE) study in optimally doped $YBa_2Cu_3O_{7-\delta}$ was performed in 1987, but no appreciable OIE on $T_c$ could be detected [32]. From this finding, the majority of researchers concluded erroneously that the electron–phonon interaction, or, more generally, lattice effects, are not responsible for superconductivity in the cuprates, and alternative models—mainly of purely electronic origin—were proposed to explain the high-temperature superconductivity in the cuprates. Consequently, lattice effects were almost completely ignored. However, soon after the first OIE study [32], it was demonstrated that all cuprate superconductors exhibit a finite OIE on $T_c$ at all doping levels, increasing substantially with reduced doping (see, e.g., [33,34]), which is a generic trend, as shown by the examples presented in Figure 3. These IE results clearly indicate that lattice effects are essential to understand the basic physics of cuprate high-temperature superconductors.

Having the JT polaron concept in mind, K.A. Müller was convinced early on that the isotope effect also plays a vital role in understanding the nature of high-temperature superconductity in the cuprates [35]. Consequently, in 1990, he initiated a new project, "Isotope Effects in Cupate Superconductors", at the University of Zurich [36–39]. The primary aim of this project was to perform a so-called site-selective oxygen isotope effect (SOIE) study on $T_c$ in optimally doped $YBa_2Cu_3O_{7-\delta}$ [40]: Which oxygen atoms (planar (p), apical (a) or chain (c) oxygens) in the lattice contribute most to the OIE shift of $T_c$? The results of this investigation, together with complementary SOIE studies of $Y_{1-x}Pr_xBa_2Cu_3O_{7-\delta}$ ($x = 0, 0.3, 0.4$) [41,42], are displayed in Figure 4. It is obvious from the figure that, for all doping levels $x$, the main contribution ($\geq$80%) to the isotope shift of $T_c$ arises from the oxygen atoms in the $CuO_2$ planes. This is opposite to what was expected by K.A. Müller in his original proposal, where he attributed large anharmonicity to the apical oxygen ions and a major contribution of them to the OIE on $T_c$ [35].

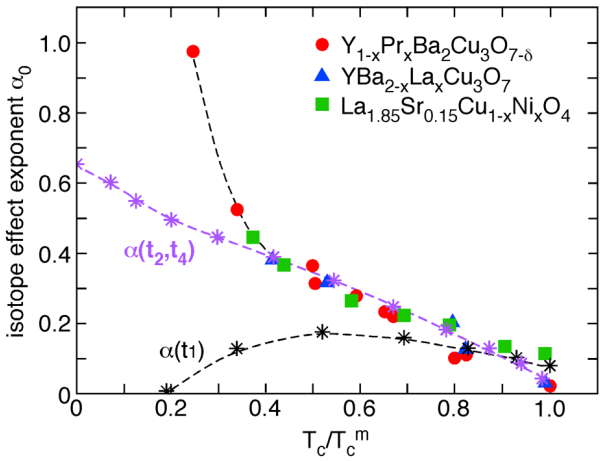


**Figure 3.** Oxygen isotope effect exponent $\alpha_O$ for various families of cuprate high-temperature superconductors (red, blue and green data points) vs. reduced temperature $T_c/T_c^m$ ($T_c^m$ is the maximum $T_c$ for a particular family of cuprates). This behavior of $\alpha_O(T_c/T_c^m)$ is generic for all families of cuprate superconductors. The black stars refer to the calculated $\alpha$ when only the nearest neighbor hopping integral ($t_1$) is renormalized. The purple stars are theoretically derived where both the second nearest neighbor ($t_2$) and the interplanar ($t_4$) hopping integrals are renormalized. Note that in order to achieve the depicted dependence of $\alpha$ as a function of $T_c/T_c^m$, the inclusion of $t_4$ is essential, thereby emphasizing the 3D nature of superconductivity. (From [43]).

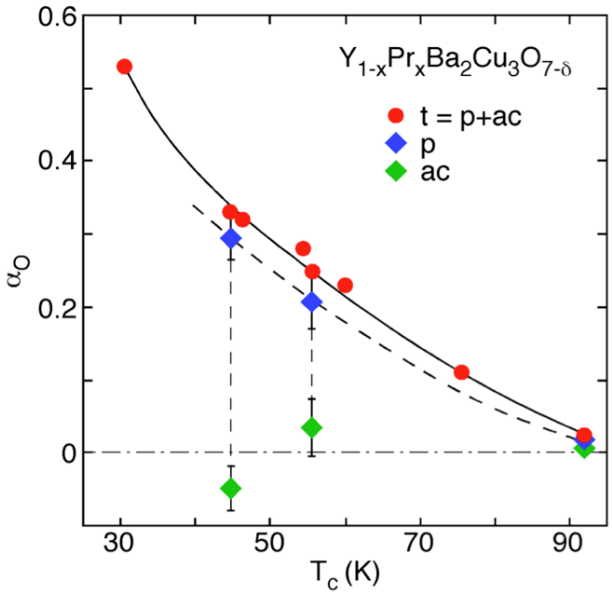


**Figure 4.** Total (t) and partial (p,ac) oxygen isotope exponent $\alpha_O$ as a function of $T_c$ for $Y_{1-x}Pr_xBa_2Cu_3O_{7-\delta}$ (t = total: all oxygen sites, p: planar oxygen sites, ac: apex and chain oxygen sites). Solid and dashed lines are visual guides. (After [36]).

Besides the OIE and SOIE on $T_c$ discussed above, doping-dependent unconventional OIEs were also observed on various physical quantities, such as the magnetic penetration depth $\lambda$, the spin-glass transition temperature $T_g$, the spin-stripe ordering tempertaure $T_{so}$ and the pseudogap temperature $T^*$ [36–39,43–45]. In the following, we only discuss the OIEs on $\lambda$ and $T^*$, which both demonstrate the polaronic character of the supercarriers in the cuprates.

In weak-coupling BCS theory (Migdal adiabatic approximation), the effective mass $m^*$ of the supercarriers is independent of the mass $M$ of the lattice atoms. However, in the JT polaron concept, the adiabatic approximation is no more fulfilled, and $m^*$ depends on

$M$. A direct test of this is the observation of an IE on the magnetic penetration depth $\lambda$, which is absent in a weak-coupling BCS superconductor. For a cuprate high-temperature superconductor, the zero-temperature in-plane magnetic penetration depth $\lambda_{ab}$ is given by [36]:

$$\lambda_{ab}(0) = \sqrt{\frac{1}{\mu_0 e^2}\frac{m^*_{ab}}{n_s}}, \tag{17}$$

where $n_s$ is the superconducting carrier density and $m^*_{ab}$ is the in-plane effective mass of the carriers. It is convenient to express the OIE on $\lambda_{ab}(0)$ in terms of the in-plane superfluid density $\rho_s \propto 1/\lambda^2_{ab}(0)$, yielding:

$$\Delta\rho_s/\rho_s = \Delta\lambda^{-2}_{ab}(0)/\lambda^{-2}_{ab}(0) = \Delta n_s/n_s - \Delta m^*_{ab}/m^*_{ab}. \tag{18}$$

This implies that any OIE shift of the superfluid density $\rho_s$ arises from an OIE shift of $n_s$ and/or $m^*_{ab}$.

OIE studies of the magnetic penetration were performed on a number of families of cuprates by means of different experimental techniques (magnetization measurements, torque magnetometry, muon-spin rotation ($\mu$SR)) and on various kinds of samples (fine-grained powder samples, microcrystals, thin films) (see, e.g., [36–39]). All these studies show a clear OIE on the magnetic penetration depth, which increases with decreasing doping (decreasing $T_c$) for all investigated cuprates. As an example, we show in Figure 5 some of these results obtained on microcrystals of underdoped $La_{2-x}Sr_xCuO_4$ ($x = 0.080, 0.086$) using high-sensitivity torque magnetometry [46]. A large OIE on the in-plane magnetic penetration depth $\lambda_{ab}(0)$ was detected: $\Delta\lambda^{-2}_{ab}(0)/\lambda^{-2}_{ab}(0) = -9(3)\%$ for $x = 0.080$ and $-7(1)\%$ for $x = 0.086$, respectively [46]. Moreover, a site-selective OIE (SOIE) study of $\lambda_{ab}$ in underdoped $Y_{0.6}Pr_{0.4}Ba_2Cu_3O_{7-\delta}$ revealed that the planar oxygens mainly contribute ($\simeq 100\%$) to the OIE shifts of $T_c$ and $\lambda_{ab}$ (see also Figure 4) [42].

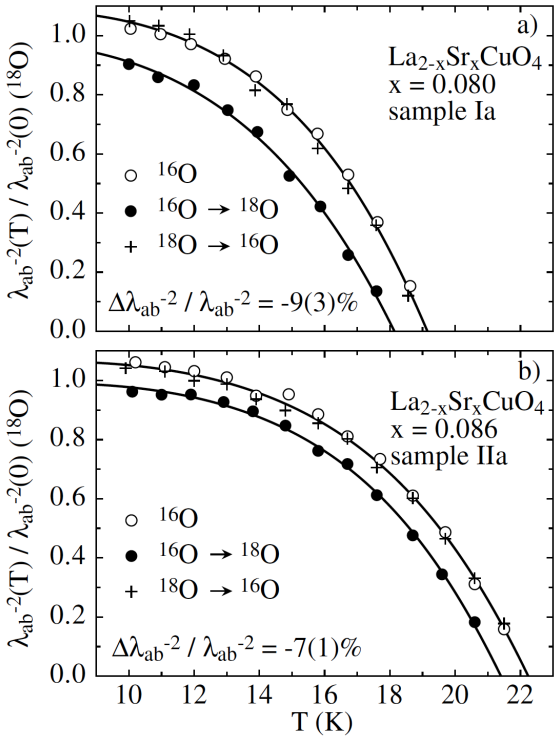


**Figure 5.** Normalized in-plane superfluid density $\Delta\lambda^{-2}_{ab}(0)/\lambda^{-2}_{ab}(0)$ for microcrystals of $La_{2-x}Sr_xCuO_4$: (**a**) $x = 0.080$; (**b**) $x = 0.086$. The reproducibility of the oxygen exchange procedure was checked by backexchange (crosses). (Reprinted with permission from Ref. [46]. Copyright 2000 APS).

For comparision, the boron isotope ($^{10}B/^{11}B$) effect on $T_c$ and the magnetic penetration depth $\lambda$ were also investigated in the conventional two-gap superconductor $MgB_2$ [47]. As expected, a substantial isotope effect on $T_c$ was observed, but no isotope effect on $\lambda$ could be detected in this BCS-type superconductor.

It is generally accepted that the pseudogap temperature $T^*$ plays a crucial role in understanding the complex physics of cuprates. However, from an experimental point of view, the temperature $T^*$ is ill-defined. It is more a "crossover temperature" rather than a phase transition temperature, and depends on the time and length scales of the experimental technique (see, e.g., [48]). Here, we define $T^*$ as the temperature where deviations from the average local structure set in (charge ordering or charge-stripe ordering temperature). Note that, for this definition of $T^*$, magnetic effects are unimportant. Thus, a possible OIE on $T^*$ reflects the presence of lattice/polaron effects. Up to now, several studies on the OIE on $T^*$ on different cuprate systems have been performed by means of X-ray absorption near-edge structure (XANES) studies [48,49] and neutron crystal-field spectroscopy (NCFS) studies [50–54]. All these studies show a large negative OIE on $T^*$. The results of all present OIE studies of $T^*$ and $T_c$ of $La_{2-x}Sr_xCuO_4$ obtained by XANES [48,49] together with the NCFS results for $La_{1.96-x}Ho_{0.04}Sr_xCuO_4$ [53,54] are presented in Figure 6. Note that the OIE exponent $\alpha_{T^*}$ is sign-reversed to $\alpha_{T_c}$ and increases almost linearly from $\alpha_{T^*} \approx -5$ to $-0.6$ with increasing doping $x$. On the other hand, the doping dependence of the OIE exponent $\alpha_{T_c}$ shows the characteristic behavior with the anomaly at $x \simeq 1/8$ (Figure 6). Moreover, $T^*(x)$ decreases linearly with increasing $x$ with different slopes for $^{16}O$ and $^{18}O$ (see Figure 6a). The limit $T^* = 0$ K is tentatively identified as a "quantum critical point $x_c$" [55,56]. Since $x_c$ exhibits a pronounced OIE [48], this "special point" thus cannot be of purely electronic origin, as widely assumed.

Furthermore, additional NCFS studies of the $^{63}Cu/^{65}Cu$ isotope effect of $T^*$ in double-layer $HoBa_2Cu_4O_8$ [52] and in single-layer $La_{1.81}Ho_{0.04}Sr_{0.15}CuO_4$ [53] revealed a large negative isotope shift of $T^*$ for the double-layer compound, but no isotope shift for the single-layer compound. Whereas oxygen and copper JT-type modes are both relevant for the double-layer compound, the so-called umbrella-type copper modes are absent in the single-layer compound, consistent with the observed oxygen and copper isotope effects on $T^*$ [53].

A theoretical explanation of the above-described IE has been given in [43], where the renormalizations of the hopping integrals through polaron formation have been investigated in detail. In order to reproduce the band structure of cuprates with a minimum model, the nearest ($t_1$) and second nearest ($t_2$) neighbor hopping together with the interplanar ($t_4$) one are sufficient [57]. Their exponential narrowing has been treated variationally and as a function of isotopic replacement. As depicted in Figure 3, only $t_2$ and $t_4$ contribute correctly to the IE, whereas $t_1$ is counterproductive. By combining these results with the corresponding lattice displacements (Figure 7), it is apparent that only the $Q_2$-type lattice mode is essentially involved in the OIE, thereby confirming the original viewpoint of JT polaron formation. Note that the interplanar hopping $t_4$ plays an important role in the correct derivation of the OIE on $T_c$ (see Figure 3), and thus demonstrates that the CuO planes are not the only relevant structural elements for HTSC, but that the interplanar coupling (3D) needs to be included as well.

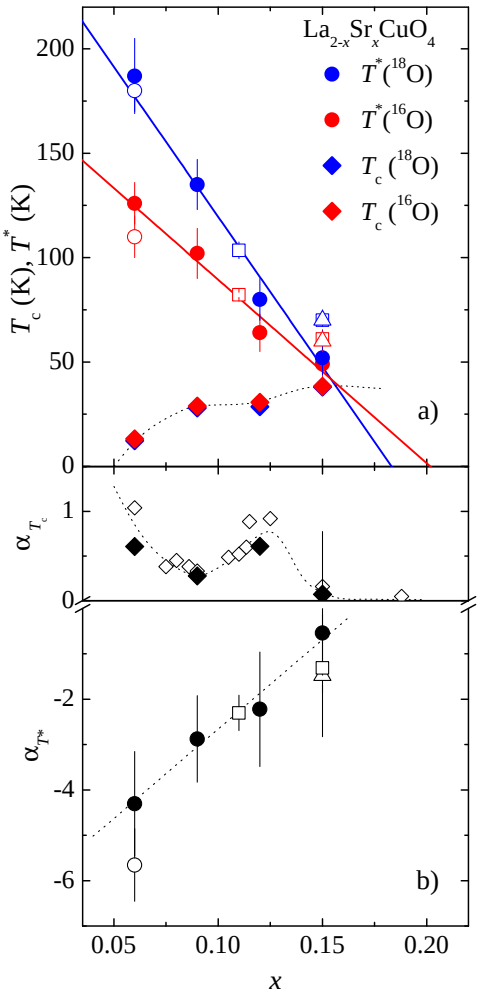


**Figure 6.** (**a**) The superconducting transition temperature $T_c$ and the pseudogap temperature $T^*$ of $La_{2-x}Sr_xCuO_4$ as a function of doping $x$ for $^{16}O$ (red symbols) and $^{18}O$ (blue symbols). The solid lines are obtained from a linear fitting. The dashed line is a visual guide. The data are results from XANES and NCFS experiments (see [48]). (**b**) Doping dependence of the isotope effect exponent $\alpha_{T_c}$ and $\alpha_{T^*}$ for $La_{2-x}Sr_xCuO_4$. The data of $\alpha_{T^*}$ are obtained by various XANES and NCFS experiments and the data of $\alpha_{T_c}$ are from magnetization measurements (see [48]). The dashed lines are a visual guide. (Reprinted with permission from Ref. [48]. Copyright 2017 APS).

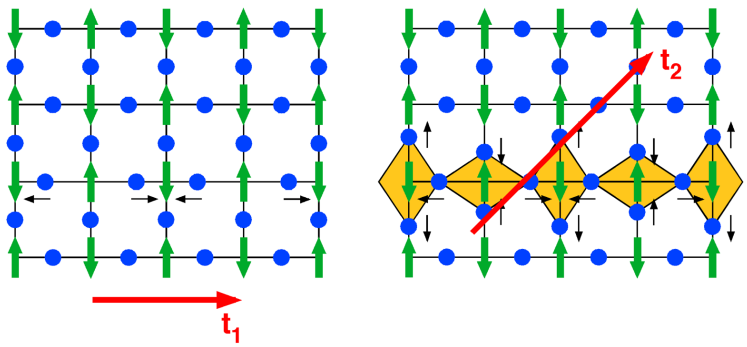


**Figure 7.** The relevant ionic displacements in the $CuO_2$ plane dominated by the nearest ($t_1$) and or second nearest ($t_2$) hopping integrals, giving rise to a $Q_2$-type phonon mode visualized by the yellow areas. Note that the interplanar hopping integral $t_4$ is not depicted in this 2D scheme, even though it is important for the OIE on $T_c$, as is evident from Figure 3. (From [43]).

In the following, we concentrate on the correlated effect arising from the lattice degrees of freedom and evaluate its response to polaron formation. Since the above-described isotope experiments support directly the eminent role played by the lattice, it is of importance to see which effects result in the lattice response. Polaron formation has coupled consequences for the electronic and lattice degrees of freedom. While, as pointed out above, the electronic hopping is renormalized by it, the lattice displacements experience a rigid, electronically induced shift. This means that the lattice-related Hamiltonian transforms to [12]:

$$\tilde{H} = \sum_{q,j} \hbar\tilde{\omega}_{q,j} \, (\tilde{b}^{+}_{q,j} \, \tilde{b}_{q,j} + 1/2) \tag{19}$$

with

$$\tilde{b}^{+}_{q} = b^{+}_{q} + \sum_{q} \gamma_i(q) \, c^{+}_{i} \, c_i \, , \;\; \tilde{b}_{q} = b_{q} + \sum_{q} \gamma_i(q) \, c^{+}_{i} \, c_i \, , \tag{20}$$

where the momentum $q$ and branch $j$-dependent renormalized frequencies $\tilde{\omega}_{q,j}$ are given by [58,59]:

$$\tilde{\omega}^2_{q,j} = {\omega^{(0)}_{q,j}}^2 - \frac{\gamma^2_{q,j}}{N(E_F)} \sum_{k} \frac{1}{\varepsilon(k)} \, \tanh \frac{\varepsilon(k)}{k_B T} \tag{21}$$

with $\varepsilon(k)$ being the Fourier transform of the site representation and $\omega^{(0)}_{q,j}$ the bare unrenormalized frequency. The coupling to the electronic degrees of freedom introduces an important temperature-dependent softening of this coupled mode, which is no longer a pure lattice mode, but represents the combined distortion of lattice and electronic degrees of freedom. The momentum $k$-dependent electronic dispersion is given by:

$$\varepsilon(k) = -2t_1[\cos(k_x a) + \cos(k_y b)] + 4t_2 \cos(k_x a) \, \cos(k_y b) \mp t_4[\cos(k_x a) - \cos(k_y b)]^2 - \mu, \tag{22}$$

where $t_1$, $t_2$ and $t_4$ account for the hopping integrals defined above, and $\mu$ is the chemical potential, which controls the band filling. Below $T_c$, $\varepsilon(k)$ has to be replaced by $E(k) = \sqrt{\varepsilon(k)^2 + \Delta(k)^2}$, where $\Delta(k)$ is the superconducting energy gap, which can be of $d$-wave or $s$-wave symmetry, or be represented by a mixed $(s+d)$-wave order parameter, as suggested from $\mu$SR experiments [21–23] discussed above (see Figure 1). As mentioned above, $\tilde{\omega}^2_{q,j}$ gains a substantial temperature dependence due to its coupling to the charge and softens with decreasing temperature at finite momentum $q$, which defines the periodicity of a modulated structure [58,59]. When this softening is complete, a dynamic superstructure in the polaron spatial distribution appears, which we identify here with the so-called stripe pseudogap phase [60,61]. Within this description, the onset temperature $T^*$ is determined by the coupling constant $\gamma$ and the energy of the unrenormalized mode frequency ${\omega^{(0)}_{q,j}}^2$, which is given by the following implicit relation:

$${\omega^{(0)}_{q,j}}^2 = \frac{\gamma^2_{q,j}}{N(E_F)} \sum_{k} \frac{1}{\varepsilon(k)} \, \tanh \frac{\varepsilon(k)}{k_B T^*} \tag{23}$$

$\gamma$ is the relevant control parameter, which systematically grows upon approaching the underdoped regime, where localization sets in and a metal to insulator transition takes place. Note that the pseudogap temperature $T^*$ is isotope-dependent through the coupled effects of the isotope dependence of the bare lattice frequency and the polaronic renormalizations of the band energies. The isotope effect on $T^*$ is sign-reversed as compared to the one on $T_c$, and it is huge, in full agreement with the XANES and NCFS experiments presented above (see Figure 6), demonstrating the importance of polaron formation. Above $T^*$, the polarons are transient, dynamic and randomly distributed over the lattice forming around the doped hole, since the extra charge introduced by doping induces a local lattice distortion, which is tied to this charge. At high temperatures, the dynamics of these objects exhibit rather high frequencies. Upon approaching $T^*$, their dynamics slow down and are almost frozen at $T^*$. Below $T^*$, the polarons become persistent, but are still dynamic with high frequencies

and confined to the new patterned modulations, which are determined by the momentum at which the local dynamics freeze in. The relative mean square displacement $\sigma^2$ of the copper–oxygen distance [58,59] as a function of temperature for $\gamma^2 = 0.25$ and $T_c = 40$ K is shown in Figure 8.

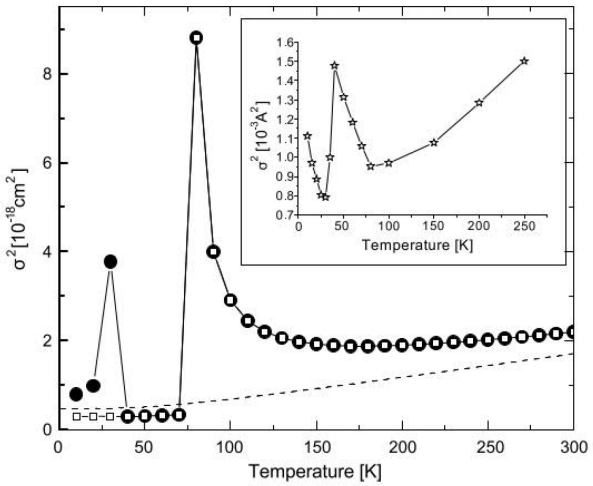


**Figure 8.** Calculated temperature dependence of the mean square displacement $\sigma^2$ for an *s*-wave superconductor (filled circles) and a *d*-wave superconductor (open squares). The inset shows experimental EXAFS data for $La_{1.85}Sr_{0.15}CuO_4$ [62]. (From [58]).

The filled black circles/open black squares refer to an *s*-wave and a *d*-wave order parameter, respectively. For comparison, the bare unrenormalized mean square displacement ($\gamma = 0$) is added (dashed line). The inset shows the experimental data for $La_{1.85}Sr_{0.15}CuO_4$ [62]. Note that, in the calculations, no damping or artificial line width broadening was introduced in order to minimize the number of parameters. As is apparent from Figure 8, the experimental data can only be reproduced by including an *s*-wave order parameter that correctly models the dip/hump structure below $T^*$ and is absent in a pure *d*-wave scenario.

## 7. Concluding Remarks

In the above, we have provided various experimental results that highlight the role of special lattice effects in cuprate high-temperature superconductors. All of these have their origin in the JT polaron concept, which is based on JT physics in combination with its itinerant character, the JT polaron. One might argue that the picture is incomplete if we ignore spin fluctuations, electronic effects and considering their influence for the pairing interaction. However, in our opinion, the essential interactions must lie in this approach, since consistent explanations for the discussed experimental results are absent in any of the alternative models. Thereby, we close the circle initiated by K.A. Müller, who started his successful career for new oxide superconductors with this concept in mind.

Finally, we wish to address the consequences for further work and searches regarding high-temperature superconductivity. Following our above remarks, a reasonable undertaking would be to look for transition metal oxides or chalcogenides where the metal ion should be a JT active one with the tendency to valence instability, thus ensuring that the ground state is intrinsically heterogeneous. In combination with the unconventional large polarizability of oxygen, respectively chalcogen ions, fluctuating charge transfer is enabled, which enhances the charge–lattice coupling locally and allows for unusual lattice anomalies in conjunction with possible pairing instabilities. In this context, it is important to re-emphasize that the electron–lattice interaction considered in our approach is *not* the conventional BCS electron–phonon interaction, which is long-range, but a local one outside the Born–Oppenheimer approximation. This leads to the discussed unconventional

isotope effects, which are typically overlooked or even ignored in purely electronic or spin-fluctuation-based pairing scenarios. Furthermore, and as outlined above, combined order parameters are a consequence that not only leads to agreement with puzzling experiments, but also accounts for the complexity in the electronic structure of cuprates, often avoided in strongly simplified alternative procedures.

**Author Contributions:** Both authors have contributed equally to all parts of the paper. All authors have read and agreed to the published version of the manuscript.

**Funding:** This research received no external funding.

**Data Availability Statement:** All data are published in research journals.

**Conflicts of Interest:** The authors declare no conflict of interest.

## References


1. Bednorz, J.G.; Müller, K.A. Possible High $T_c$ Superconductivity in the Ba-La-Cu-O System. *Z. Phys. B-Condens. Matter.* **1986**, *64*, 189–193. [CrossRef]
2. Bardeen, J.; Cooper, L.N.; Schrieffer, J.R. Microscopic Theory of Superconductivity. *Phys. Rev. B* **1957**, *106*, 162–164. [CrossRef]
3. Bardeen, J.; Cooper, L.N.; Schrieffer, J.R. Theory of Superconductivity. *Phys. Rev. B* **1957**, *108*, 1175–1204. [CrossRef]
4. Maxwell, E. Isotope Effect in the Superconductivity of Mercury. *Phys. Rev.* **1950**, *78*, 477. [CrossRef]
5. Reynolds, C.A.; Serin, B.; Wright, W.H.; Nesbitt, L.B. Superconductivity of Isotopes of Mercury. *Phys. Rev.* **1950**, *78*, 487. [CrossRef]
6. Jahn, H.; Teller, E. Stability of Degenerate Electronic States in Polyatomic Molecules. *Phys. Rev.* **1936**, *49*, 874–880.
7. Jahn, H.A.; Teller, E. Stability of Polyatomic Molecules in Degenerate Electronic States I-Orbital Degeneracy. *Proc. R. Soc. A* **1937**, *161*, 220–235.
8. Höck, K.-H.; Nickisch, H.; Thomas, H. Jahn-Teller effect in itinerant electron systems: The Jahn-Teller polaron. *Helv. Phys. Acta* **1983**, *56*, 237–243.
9. Holstein, T. Studies of polaron motion: Part I. The molecular-crystal model. *Ann. Phys.* **1959**, *8*, 325–342. [CrossRef]
10. Alexandrov A.S.; Mott, N.F. Bipolarons. *Rep. Progr. Phys.* **1994**, *57*, 1197–1288. [CrossRef]
11. Alexandrov, A.S.; Mott, N.F. *Polarons and Bipolarons*; World Scientific Publishing Company: Singapore, 1996; pp. 1–204.
12. Lang, I.G.; Firsov, Y.A. Kinetic Theory of Semiconductors with Low Mobility. *Zh. Eksp. Teor. Fiz.* **1962**, *43*, 1843–1860. (In Russian)
13. Müller, K.A. Essential Heterogeneities in Hole-Doped Cuprate Superconductors. In *Superconductivity in Complex Systems*; Structure and Bonding 114; Müller, K.A., Bussman-Holder, A., Eds.; Springer: Berlin/Heidelberg, Germany, 2005; pp. 1–11.
14. Müller, K.A. Possible coexistence of *s*- and *d*-wave condensates in copper oxide superconductors. *Nature* **1995**, *377*, 133–135 . [CrossRef]
15. Bianconi, A.; Saini, N.L.; Lanzara, A.; Missori, M.; Rossetti, T.; Oyanagi, H.; Yamaguchi, H.; Oka, K.; Ito, T. Determination of the Local Lattice Distortions in the $CuO_2$ Plane of $La_{1.85}Sr_{0.15}CuO_4$. *Phys. Rev. Lett.* **1996**, *76*, 3412–3415. [CrossRef]
16. Kresin V.Z.; Wolf, S.A. Colloquium: Electron-lattice interaction and its impact on high $T_c$ superconductivity. *Rev. Mod. Phys.* **2009**, *81*, 481–501. [CrossRef]
17. Wollman, D.A.; Van Harlingen, D.J.; Lee, W.C.; Ginsberg, D.M.; Leggett, A.J. Experimental determination of the superconducting pairing state in YBCO from the phase coherence of YBCO-Pb dc SQUIDs. *Phys. Rev. Lett.* **1993**, *71*, 2134–2137. [CrossRef] [PubMed]
18. Tsuei, C.C.; Kirtley, J.R.; Chi, C.C.; Yu-Jahnes, L.S.; Gupta, A.; Shaw, T.; Sun, J.Z.; Ketchen, M.B. Pairing Symmetry and Flux Quantization in a Tricrystal Superconducting Ring of $YBa_2Cu_3O_{7-\delta}$. *Phys. Rev. Lett.* **1994**, *73*, 593–596. [CrossRef]
19. Brawner, D.A.; Ott, H.R. Evidence for an unconventional superconducting order parameter in $YBa_2Cu_3O_{6.9}$. *Phys. Rev. B* **1994**, *50*, 6530–6533. [CrossRef]
20. Müller, K.A.; Keller, H. *s* and *d* Wave Symmetry Components in High-Temperature Cuprate Superconductors. In *High-$T_c$ Superconductivity 1996: Ten Years after the Discovery*; Kaldis, E., Liarokapis, E., Müller, K.A., Eds.; Kluwer Academic Publishers: Dordrecht, The Netherlands; Boston, MA, USA; London, UK, 1997; pp. 7–29.
21. Khasanov, R.; Shengelaya, A.; Maisuradze, A.; La Mattina, F.; Bussmann-Holder, A.; Keller, H.; Müller, K.A. Experimental evidence for two gaps in the high-temperature $La_{1.83}Sr_{0.17}CuO_4$ superconductor. *Phys. Rev. Lett.* **2007**, *98*, 057007-1. [CrossRef]
22. Khasanov, R.; Strässle, S.; Di Castro, D.; Masui, T.; Miyasaka, S.; Tajima, S.; Bussmann-Holder, A.; Keller, H. Multiple gap symmetries for the order parameter of cuprate superconductors from penetration depth measurements. *Phys. Rev. Lett.* **2007**, *99*, 237601-1. [CrossRef] [PubMed]
23. Khasanov, R.; Shengelaya, A.; Karpinski, J.; Bussmann-Holder, A.; Keller, H.; Müller, K.A. $s-$wave symmetry along the *c*-axis and $s+d$ in-plane superconductivity in bulk $YBa_2Cu_4O_8$. *J. Supercond. Nov. Magn.* **2008**, *21*, 81–85. [CrossRef]
24. Sun, A.G.; Gajewski, D.A.; Maple, M.B.; Dynes, R.C. Observation of Josephson pair tunneling between a high-$T_c$ cuprate ($YBa_2Cu_3O_{7-\delta}$) and a conventional superconductor (Pb). *Phys. Rev. Lett.* **1994**, *72*, 2267–2270. [CrossRef]
25. Bussmann-Holder, A.; Khasanov, R.; Shengelaya, A.; Maisuradze, A.; La Mattina, F.; Keller, H.; Müller, K.A. Mixed order parameter symmetries in cuprate superconductors. *Europhys. Lett.* **2007**, *77*, 27002. [CrossRef]

26. Müller, K.A. On the macroscopic *s*- and *d*-wave symmetry in cuprate superconductors. *Philos. Mag. Lett.* **2002**, *82*, 279–288. [CrossRef]
27. Iachello, F. A model of cuprate superconductors based on the analogy with atomic nuclei. *Philos. Mag. Lett.* **2002**, *82*, 289–295. [CrossRef]
28. Khasanov, R.; Shengelaya, A.; Brütsch, R.; Keller, H. Suppression of the *s*-wave Order Parameter Near the Surface of the Infinite-Layer Electron-Doped Cuprate Superconductor $Sr_{0.9}La_{0.1}Cu_2$. *Condens. Matter* **2020**, *5*, 50. [CrossRef]
29. Suhl, H.; Matthias, B.T.; Walker, L.R. Bardeen-Cooper-Schrieffer Theory of Superconductivity in the Case of Overlapping Bands. *Phys. Rev. Lett.* **1959**, *3*, 552–555. [CrossRef]
30. Moskalenko, V. Superconductivity in metals with overlapping energy bands. *Fiz. Metal. Met.* **1959**, *8*, 2518–2529.
31. Micnas, R.; Robaszkiewicz, S.; Bussmann-Holder, A. Two-Component Scenarios for Non-Conventional (Exotic) Superconductors. In *Superconductivity in Complex Systems*; Structure and Bonding 114; Müller, K.A., Bussmann-Holder, A., Eds.; Springer: Berlin/Heidelberg, Germany, 2005; pp. 13–69.
32. Batlogg, B.; Cava, R.J.; Jayaraman, A.; van Dover, R.B.; Kourouklis, G.A.; Sunshine, S.; Murphy, D.W.; Rupp, L.W.; Chen, H.S.; White, A.; et al. Isotope Effect in the High-Tc Superconductors $Ba_2YCu_3O_7$ and $Ba_2EuCu_3O_7$. *Phys. Rev. Lett.* **1987**, *58*, 2333–2336. [CrossRef]
33. Franck, J.P.; Jung, J.; Mohamed, A.K.; Gygax, S.; Sproule, G.I. Observation of an oxygen isotope effect in superconducting $(Y_{1-x}Pr_x)Ba_2Cu_3O_{7-\delta}$. *Phys. Rev. B* **1991**, *44*, 5318–5321. [CrossRef]
34. Franck, J.P. Experimental studies of the isotope effect in high temperature superconductors. In *Physical Properties of High Temperature Superconductors IV*; Ginsberg, D.M., Ed.; World Scientific: Singapore, 1994; pp. 189–293.
35. Müller, K.A. On the oxygen isotope effect and apex anharmonicity in high-$T_c$ cuprates. *Z. Phys. B-Condens. Matter* **1990**, *80*, 193–201. [CrossRef]
36. Keller, H. Unconventional Isotope Effects in Cuprate Superconductors. In *Superconductivity in Complex Systems*; Structure and Bonding 114; Müller, K.A., Bussmann-Holder, A., Eds.; Springer: Berlin/Heidelberg, Germany, 2005; pp. 143–169.
37. Zhao, G.M.; Conder, K.; Keller, H.; Müller, K.A. Oxygen isotope effects in $La_{2-x}Sr_xCuO_4$: Evidence for polaronic charge carriers and their condensation. *J. Phys. Condens. Matter* **1998**, *10*, 9055–9066. [CrossRef]
38. Zhao, G.M.; Keller, H.; Conder, K. Unconventional isotope effects in the high-temperature cuprate superconductors. *J. Phys. Condens. Matter* **2001**, *13*, R569–R587. [CrossRef]
39. Bussmann-Holder, A.; Keller, H. From $SrTiO_3$ to Cuprates and Back to $SrTiO_3$: A Way Along Alex Müller's Scientific Career. *Condens. Matter* **2021**, *6*, 2. [CrossRef]
40. Zech, D.; Keller, H.; Conder, K.; Kaldis, E.; Liarokapis, E.; Poulakis, N.; Müller, K.A. Site-selective oxygen isotope effect in optimally doped $YBa_2Cu_3O_{6+x}$. *Nature* **1994**, *371*, 681–683. [CrossRef]
41. Zhao, G.M.; Ager, J.W., III; Morris, D.E. Site dependence of large oxygen isotope effect in $Y_{0.7}Pr_{0.3}Ba_2Cu_3O_{6.97}$. *Phys. Rev. B* **1996**, *54*, 14982–14985. [CrossRef]
42. Khasanov, R.; Shengelaya, A.; Morenzoni, E.; Angst, M.; Conder, K.; Savić, I.M.; Lampakis, D.; Liarokapis, E.; Tatsi, A.; Keller, H. Site-selective oxygen isotope effect on the magnetic field penetration depth in underdoped $Y_{0.6}Pr_{0.4}Ba_2Cu_3O_{7-\delta}$. *Phys. Rev. B* **2003**, *68*, 220506. [CrossRef]
43. Keller, H.; Bussmann-Holder, A.; Müller, K.A. Jahn-Teller physics and high-$T_c$ superconductivity. *Mater. Today* **2008**, *11*, 38–46. [CrossRef]
44. Khasanov, R.; Shengelaya, A.; Di Castro, D.; Morenzoni, E.; Maisuradze, A.; Savić, I.M.; Conder, K.; Pomjakushina, E.; Bussmann-Holder, A.; Keller, H. Oxygen isotope effect on the superconducting transition and magnetic states within the phase diagram of $Y_{1-x}Pr_xBa_2Cu_3O_{7-\delta}$. *Phys. Rev. Lett.* **2008**, *101*, 077001. [CrossRef]
45. Guguchia, Z.; Khasanov, R.; Bendele, M.; Pomjakushina, E.; Conder, K.; Shengelaya, A.; Keller, H. Negative Oxygen Isotope Effect on the Static Spin Stripe Order in Superconducting $La_{2-x}Ba_xCuO_4$ ($x = 1/8$) Observed by Muon-Spin Rotation. *Phys. Rev. Lett.* **2014**, *113*, 057002. [CrossRef]
46. Hofer, J.; Conder, K.; Sasagawa, T.; Zhao, G.M.; Willemin, M.; Keller, H.; Kishio, K. Oxygen-isotope effect on the in-plane penetration depth in underdoped $La_{2-x}Sr_xCuO_4$ single crystals. *Phys. Rev. Lett.* **2000**, *84*, 4192–4195. [CrossRef]
47. Di Castro, D.; Angst, M.; Eshchenko, D.G.; Khasanov, R.; Roos, J.; Savić, I.M.; Shengelaya, A.; Budko, S.L.; Canfield, P.C.; Conder, K.; et al. Absence of a boron isotope effect in the magnetic penetration depth of $MgB_2$. *Phys. Rev. B* **2004**, *70*, 014519. [CrossRef]
48. Bendele, M.; von Rohr, F.; Guguchia, Z.; Pomjakushina, E.; Conder, K.; Bianconi, A.; Simon, A.; Bussmann-Holder, A.; Keller, H. Evidence for strong lattice effects as revealed from huge unconventional oxygen isotope effects on the pseudogap temperature in $La_{2-x}Sr_xCuO_4$. *Phys. Rev. B* **2017**, *95*, 014514. [CrossRef]
49. Lanzara, A.; Zhao, G.-m.; Saini, N.L.; Bianconi, A.; Conder, K.; Keller, H.; Müller, K.A. Oxygen-isotope effect of the charge-stripe ordering temperature in $La_{2-x}Sr_xCuO_4$ from x-ray absorption spectroscopy. *J. Phys. Condens. Matter* **1999**, *11*, L541–L546. [CrossRef]
50. Rubio Temprano, D.; Mesot, J.; Janssen, S.; Conder, K.; Furrer, A.; Mutka, H.; Müller, K.A. Large Isotope Effect on the Pseudogap in the High-Temperature Superconductor $HoBa_2Cu_4O_8$. *Phys. Rev. Lett.* **2000**, *84*, 1990–1993. [CrossRef] [PubMed]
51. Rubio Temprano, D.; Furrer, A.; Conder, K.; Mutka, H. A neutron crystal-field study of the pseudogap in the underdoped high $T_c$ superconductor $HoBa_2Cu_4^{18}O_8$. *Phys. B* **2000**, *276–278*, 762–763. [CrossRef]

52. Rubio Temprano, D.; Mesot, J.; Janssen, S.; Conder, K.; Furrer, A.; Sokolov, A.; Trounov, V.; Kazakov, S.M.; Karpinski, J.; Müller, K.A. Large copper isotope effect on the pseudogap in the high-temperature superconductor $HoBa_2Cu_4O_8$. *Eur. Phys. J. B* **2001**, *19*, 5–8. [CrossRef]
53. Rubio Temprano, D.; Conder, K.; Furrer, A.; Mutka, H.; Trounov, V.; Müller, K.A. Oxygen and copper isotope effects on the pseudogap in the high-temperature superconductor $La_{1.81}Ho_{0.04}Sr_{0.15}CuO_4$ studied by neutron crystal-field spectroscopy. *Phys. Rev. B* **2002**, *66*, 184506. [CrossRef]
54. Häfliger, P.S.; Podlesnyak, A.; Conder, K.; Pomjakushina, E.; Furrer, A. Pseudogap of the high-temperature superconductor $La_{1.96-x}Sr_xHo_{0.04}CuO_4$ as observed by neutron crystal-field spectroscopy. *Phys. Rev. B* **2006**, *74*, 184520. [CrossRef]
55. Varma, C.M. Non-Fermi-liquid states and pairing instability of a general model of copper oxide metals. *Phys. Rev. B* **1997**, *55*, 14554–14580. [CrossRef]
56. Li, Y.; Balédent, V.; Barisić, N.; Cho, Y.; Fauqué, B.; Sidis, Y.; Yu, G.; Zhao, X.; Bourges, P.; Greven, M. Unusual magnetic order in the pseudogap region of the superconductor $HgBa_2CuO_{4+\delta}$. *Nature* **2008**, *455*, 372–375. [CrossRef]
57. Pavarini, E.; Dasgupta, I.; Saha-Dasgupta, T.; Jepsen, O.; Andersen, O.K. Band-Structure Trend in Hole-Doped Cuprates and Correlation with $T_{cmax}$. *Phys. Rev. Lett.* **2001**, *87*, 047003. [CrossRef]
58. Bussmann-Holder, A.; Keller, H.; Bishop, A.R.; Simon, A.; Müller, K.A. Polaron coherence as origin of the pseudogap phase in high temperature superconducting cuprates. *J. Supercond. Nov. Magn.* **2008**, *21*, 353–357. [CrossRef]
59. Bussmann-Holder, A.; Keller, H.; Mustre de Leon, J.; Simon, A.; Bishop, A.R.; Müller, K.A. Testing polaron coherence and the pairing symmetry by local probe methods. *J. Supercond. Nov. Magn.* **2010**, *23*, 295–299. [CrossRef]
60. Saini, N.L.; Lanzara, A.; Oyanagi, H.; Yamaguchi, H.; Oka, K.; Ito, T.; Bianconi, A. Local lattice instability and stripes in the $CuO_2$ plane of the $La_{1.85}Sr_{0.15}CuO_4$ system by polarized XANES and EXAFS. *Phys. Rev. B* **1997**, *55*, 12759–12769. [CrossRef]
61. Sharma, R.; Ogale, S.; Zhang, Z.; Liu, J.R.; Chu, W.K.; Veal, B.; Paulikas, A.; Zheng, H.; Venkatesan, T. Phase transitions in the incoherent lattice fluctuations in $YBa_2Cu_3O_{7-\delta}$. *Nature* **2000**, *404*, 736–740. [CrossRef] [PubMed]
62. Oyanagi, H.; Zhang, C.; Tsukada, A.; Naito, M. Lattice instability in high temperature superconducting cuprates probed by X-ray absorption. *J. Phys. Conf. Ser.* **2008**, *108*, 012038. [CrossRef]